Submitted to The Journal of the **Astronautical** *Sciences*

Doppler Navigation of Interplanetary Spacecraft Using Different Data Processing Modes[1]

Sam **W. Thurman[2] and** Jeff A. **Estefan[3]**

Abstract

Doppler shift measurements derived from c1oscx1-1oo]1 radio tracking of distant spacecraft by ground stations of the Deep Space Network (DSN) arc one of the principal means used for interplanetary navigation. This article describes an investigation of the navigation accuracy that can be achieved with two-way coherent X-band **(7.2** to **8.4** GHz) Doppler phase and frequency data; both theoretical and practical aspects of the. two Doppler formulations arc addressed. A new filtering strategy is also proposed, which differs from current approaches in that most of the ground system calibration errors affecting the Doppler data arc represented as filter parameters, in addition to the spacecraft trajectory parameters. Error covariance computations for applic.alien of the proposed filter to a navigation scenario derived from the *Mars Observer* mission arc provided, in order to assess the performance. that might be obtained in practice. The results indicate that with a phase formulation of the Doppler data and the new filter, navigation accuracies of 15 km at **Mars (0.05** μrad **in an angular** sense) are possible with **the** DSN's **present X-band** Doppler tracking system.

1 Originally presented at the AAS/AI AA Spaceflight Mechanics Meeting, Pasadena, California, **February 1993,** revised October **1994.**

[2]Member Technical Staff, Mission Design **Section,** Jet Propulsion Laboratory, **California** Institute of Technology, Pasadena, CA **91109.**

[3]Member Technical **Staff, Navigation** Systems Section, Jet **Prepulsion** Laboratory, California Institute **of** Technology, Pasadena, CA **91109.**

Introduction

Two-way coherent Doppler data are routinely collected as part of the tracking, telemetry, and command operations conducted by ground stations of the Deep Space Network (DSN) in support of National Aeronautics and Space Administration (NASA) and international interplanetary missions. DSN Doppler data are not direct frequency shift measurements, but counts of the number of cycles of the transmitted carrier signal relative to the received carrier signal that have accumulated since the beginning of a pass. Currently, these cycle counts are differenced to form measurements of the average Doppler shift over short t imc periods, typically 1 to 10 rein; it is these "diffcrenccd-range 1)oppler" measurements that arc actually used for navigat ion [1]. in addition to Doppler, there are several other radio metric data types collected by the DSN and used for navigation, such as two-way ranging and Delta-Differential One-Way Range (ADOR); however, Doppler data are still used extensive] y, and somet imcs exclusive] y, for navigat ion of virt ually all interplanetary spacecraft. An overview of both ground-based radio navigation and spacecraft onboard optical navigation techniques used in interplanetary missions is given by Jordan and *wood* [2].

This article investigates t wo approaches for improving Doppler navigat ion accuracy. The first of them is the usc of the original 1)oppler count as the Doppler observable, rather than the current diffcrcnccd-range 1)oppler formulation. The motivation for using counted Doppler as a navigation measurement is that the precision of these data is very high (a few millimeters at X-band frequencies); differencing the counts to form differenced-range Doppler data effective] y increases the data noise level. The utility of counted Doppler has been considered before, (as early as 1966, in an article by Curkendall [3]); given the steady improvements in the DSN tracking system over the years, the potent ial of counted Doppler merits another invest igat ion. The second proposed innovation is a sequential orbit determination filter that incorporates nearly all of the principal

ground system calibration error sources as filter parameters, in addition to the spacecraft trajectory parameters. This approach differs from the current practice, which is to represent systematic ground system error sources as *consider* parameters that are not estimated but whose effects are accounted for (i.e., "considered") in computing the error covariance of the estimated parameters.

Doppler Tracking System

A simple diagram of the DSN two-way Doppler system is shown in Fig. 1. A carrier signal of known frequency, f_T, is transmitted to the spacecraft, where it is detected, multiplied by a known turn-around ratio, K, then coherently retransmitted to the station with received frequency, f_R. In some cases the transmitted frequency is intentionally varied in a linear manner with time, a process called "ramping," in order to reduce the rate of change of the Doppler shift which must be tracked by the spacecraft's receiver. The Doppler tone of frequency $Kf_T - f_R$ is formed by mixing the transmitted and received carriers. The exciter frequency, f_T, is synthesized from a stable frequency standard, normally a hydrogen maser. A bias frequency of 1 MHz is added to the Doppler tone before it is passed to the Doppler counter, to avoid problems in the hardware associated with zero Doppler shifts and bandpass limitations, although this is not explicitly shown in Fig. 1. The axial crossings of the Doppler tone are counted and output at user-selected intervals of *0.1* to *600s* by the Doppler counter, which also contains resolver circuitry to measure the fractional part of a cycle between the last axial crossing and the current sample time.

Doppler tracking can also be performed in one-way or three-way modes. in the one-way mode, the spacecraft uses an onboard oscillator to generate a reference frequency for the downlink carrier signal. At a DSN station, the received carrier signal is compared with a local model of the spacecraft oscillator to generate data, Three-way Doppler is a special case of two-way Doppler,

with the receiving station being different from the transmitting station. in this mode, the receiving station compares a local model of the uplink carrier to the received carrier. Two-way tracking is the most common Doppler acquisition mode for navigation, as the accuracy of two-way data is much greater (factors of 10 to 1000)" than that of either one-way or three-way data.

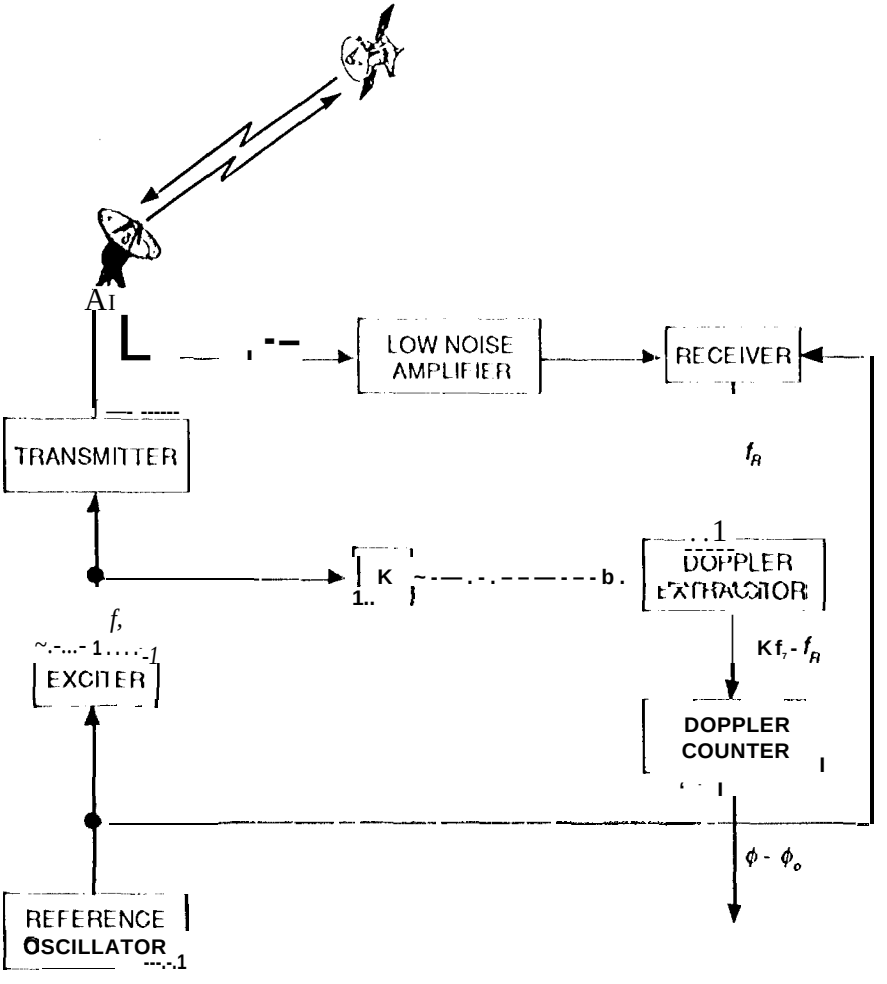

FIG. 1. DSN Two-Way Doppler Tracking System.

Doppler As A Navigation Measurement

The Doppler' counter integrates the biased Doppler frequency, yielding the phase of the Doppler

tone in cycles. The relationship between the Doppler phase and the quantities needed for a navigation measurement (e.g., time and distance) is best illustrated with a simple model of the Doppler count, which can then be used to construct approximations that provide some insight into the ability of both Doppler phase and frequency measurements to determine a spacecraft trajectory.

Observable Model

The Doppler observable model will be developed for the case in which the uplink frequency, f_T, is constant. A more detailed treatment of the general case in which f_T may be time-varying is given by Moyer [1]. With the phase of the bias frequency removed, the Doppler count, ϕ, is

$$\phi = \phi_0 + \int_{t_0}^{t} [K(f_T + \varepsilon) - f_R]dt + \eta = \phi_0 + \phi_T - \phi_R + \eta \qquad (1)$$

where

t_0 = time of spacecraft carrier signal acquisition

ϕ_0 = unknown phase offset of Doppler counter at t_0

ϕ_T = cycle count of reference frequency, Kf_T

ϕ_R = cycle count of received frequency, f_R

ε = random noise due to ground system frequency instability

η = random noise due to additive error sources

in Eq (1), the terminology of Fig. 1 is used, except as otherwise indicated. The phase offset, ϕ_0, appears because the Doppler counter cannot be set to zero precisely at time t_0. Neglecting the noise terms in Eq. (1) for the moment, the cycle counts of the reference and received frequencies in

Eq. (1) can be expressed as functions of the transmission and reception times of cycles of the carrier signal:

$$\phi_T = Kf_T(t - t_0) \tag{2}$$

$$\phi_R = Kf_T(T_t - T_0) \tag{3}$$

where

T_t = transmission time of carrier cycle received at time t

T_0 = transmission time of carrier cycle received at time t_0

Eq. (3) reflects the fact that the number of carrier cycles received and counted from time t_0 to time t must be equal to the same number of cycles that were transmitted to the spacecraft, multiplied by the spacecraft transponder turn-around ratio, K. The information contained in the Doppler count regarding the spacecraft trajectory is, therefore, embodied in the unknown transmit times T_t and T_0.

The Doppler count is currently used to form a quasi-Doppler frequency measurement known as differenced-range Doppler, denoted as f, and defined as

$$f(t_k) \triangleq (\phi_k - \phi_{k-1})/(t_k - t_{k-1}) \tag{4}$$

in Eq. (4), ϕ_k and ϕ_{k-1} are the Doppler counts at sample times t_k and t_{k-1}, respectively. With Eqs. (1) through (4), expressions for both counted and differenced-range Doppler measurements can be written in terms of transmit and receive times. The Doppler count at time t_k, designated ϕ_k, is a

function of the round-trip light time at acquisition, $_{10\text{-}7'0,}$ and the round-trip light time at sample time t_k, $t_k - T_k$:

$$\phi_k = Kf_T[(t_k - T_k) - (t_0 - T_0)] + \phi_0 \tag{5}$$

The corresponding expression for a differenced-range Doppler measurement at time t_k, designated f_k, is very similar:

$$f_k = Kf_T[(t_k - T_k) - (t_{k-1} - T_{k-1})]/(t_k - t_{k-1}) \tag{6}$$

Further development of Eqs. (5) and (6) becomes quite involved, requiring the general theory of relativity to relate the station transmit and receive times to the station-to-spacecraft range along the uplink and downlink signal paths. The interested reader should refer to the derivations given by Moyer [1] and Miller [4].

Useful analytical approximations to Eqs. (5) and (6) can be obtained by neglecting relativistic effects and round-trip light times in the station-to-spacecraft range calculations. These assumptions yield the following expressions:

$$\phi_k \approx Kf_T[2(\rho_k - \rho_0)/c] + \phi_0 \tag{7}$$

$$f_k \approx Kf_T[2(\rho_k - \rho_{k-1})/(c\,\Delta t)] \approx Kf_T(2\dot{\rho}_k/c) \tag{8}$$

where

ρ_k = station-to-spacecraft range at time t_k

ρ_0 = station-to- spacecraft range at time t_0

$\dot{\rho}_k$ = station-to-spacecraft range rate at time t_k

c = speed of light (2.99792458 X 10^8 m/s)

At = $t_k - t_{k-1}$

For X-band tracking from a DSN 34-m High Efficiency (111;1;) station, nominal values of the constants in Eqs. (7) and (8) arc f_T = 7.17 GHz, K = 880/749, and At = 60 s. Under typical conditions (carrier signal/noise ratio of 10 to 20 all]), these values translate into a phase tracking precision (1 σ) of roughl y 0.1 cycle in the presence of transmission media fluctuations [4]. For differenced-range Doppler, this yields a precision of bet wccn 1 and 2 mHz, corresponding to a range rate of ().02 to 0.04 mm/s, according to Eq. (8). For counted Doppler, Eq. (7) shows that a precision of 0.1 cycle corresponds to a precision in range change of about 2 mm. over longer time periods, the counted Doppler precision degrades because of ground system instability: over a 600 s interval, the precision is about O.15 cycle (3 mm), and over the course of a typical pass (8 to 10 hr), further degradation occurs to roughly 3 cycles (5 cm) [5],

Measurement Error Model

The effects of the measurement noise terms in Eq. (1) must now be characterized. For differenced-range Doppler, the following model is normal] y used:

$$f_k = \dot{\rho}_k + v_k \tag{9}$$

in Eq. (9), the v_k values arc samples of a zero-mean white Gaussian sequence in which each sample has constant variance and is uncorrelated with all other samples, The process incorporates both additive phase measurement errors, and errors due to ground system frequency instability that

are integrated over the count time of each observation, The variance of the ν_k samples is assumed to be constant if the count time used in constructing assumed to be constant if the count time used in constructing the data points is also constant, This approximate ion is not rigorous] y correct: since successive differenced-range Doppler data points share common values of the Doppler count, each data point is correlated with the two points adjacent to it. In practice though, it is believed that the uncorrelated measurement error assumption dots not yield significantly incorrect statistical calculations for the large Doppler data sets typically used in mission operations.

For counted Doppler, the secular nature of the phase measurement error must be taken into account, resulting in a measurement error model of the following form:

$$\phi_k \equiv (\rho_k - \rho_0) + \phi_0 + \xi_k + \eta_k \tag{10}$$

where

η_k = additive phase measurement error

ξ_k = accumulative phase measurement error

In Eq. (10), the phase offset ϕ_0, which represents the Doppler counter initialization error, is assumed to be a random bias. The η_k samples arc assumed to be a white, zero-mean Gaussian sequence with constant variance. The ξ_k values lcpre.sent the accumulated phase error induced by the integration of frequency variations by the Doppler counter. The effect of frequency instability in counter Doppler measurements was anal yzed from a theoretical standpoint by Curkendall [6]. More recently, frequency stability tests of the X-band tracking system at one of the DSN's 34-m HEF stations have been performed by K wok [7], which provide an estimate of the performance of the current system. Based on these test results and Curkendall's original analysis, it is proposed

that the phase error behavior of a hydrogen maser frequency standard distributed by temperature stabilized cables to a DSN 34-m HEF station, with a spacecraft having a round-trip light time of less than roughly 1 hr, can be approximated by a simple Brownian motion process:

$$\xi_{k+1} = \xi_k + w_k \tag{11}$$

where

w_k = Gaussian sequence representing integrated white frequency noise

The contribution of frequency noise to counted Doppler measurement error is bounded principally by the round-trip light time to the spacecraft, since this time period is the longest over which frequency noise is integrated [6]. The model given by Eq. (11) assumes that the principal source of ground system instability is high-frequency noise; performance data for the DSN frequency and timing system indicates that this is a reasonable assumption over time periods of 1 to 2 hr, but that for round-trip light times longer than this the effect of slowly varying drifts in the reference oscillator and distribution system becomes significant [8]. Therefore, Eq. (11) may be a reasonable approximation for missions out to distances at Jupiter (round-trip light time ~1.5 hr), but perhaps not any farther.

The values chosen for the parameters in Eqs. (9) through (11) to represent the DSN X-band Doppler system are given in Table 1. In Table 1, At is the count time for differenced-range Doppler data, and the time between data points for counted Doppler. The relationship between the actual and derived metric values of each parameter was obtained from Eqs. (7) and (8). The figures for the additive noise terms, v and η, were derived from an assessment of *Magellan* X-band Doppler data quality [4], and include the effects of short-term transmission media

(troposphere, ionosphere, and solar plasm) fluctuations in addition to electronic sources of error. Since X-band Doppler data are not calibrated for solar plasm effects in most missions, the frequency noise term, w, must incorporate the effect of uncalibrated secular variations in the solar plasma as well as ground system instability. Depending upon the Sun-Earth-spacecraft angle, solar plasma variations can be much 1 arger than those of the ground system, The ground system tests performed by Kwok [7] indicated that frequency stabilities of 3×10^{-15} s/s (square root Allan variance) over 1 hr have been achieved, whereas estimates of solar plasm stability over similar time scales are on the order of 10^{-14} s/s for large (>60 deg) Sun-Earth-spacecraft angles [9]. The value chosen for σ_w therefore corresponds to a frequency stability of about 10^{-14} s/s over a period of 1 hr.

TABLE 1. X-Band Doppler Measurement Error Model Parameters

Parameter	Actual Value	Metric Value
σ_v	0.37 mHz	6.6×10^{-3} mm/s
σ_η	0.13 cycle	2,4 mm
σ_w	0.12 cycle	2.1 mm
Δt	600 s	

Information Content

Thus far, it has been shown that differenced-range Doppler approximates the station-to-spacecraft range rate, assuming the short (1- to 10 rein) count times normal] y used in processing those data, and that counted Doppler is effectively the integral of range rate over a tracking pass. The station-to-spacecraft range and range rate can be expressed in simple form, by using the geometry shown in Fig. 2. The following expressions for range, ρ, and range rate, $\dot{\rho}$, are

obtained for a distant spacecraft:

$$p = r - [r_s \cos\delta \cos(\alpha_g + \lambda - \alpha) + z_s \sin\delta] \tag{12}$$

$$\begin{aligned} \dot{\rho} = \frac{d\rho}{dt} &= \dot{r} + r_s[(\omega - \dot{\alpha})\cos\delta\sin(\alpha_g + \lambda - \alpha) + \dot{\delta}\sin\delta\cos(\alpha_g + \lambda - \alpha)] - z_s\dot{\delta}\cos\delta \\ &\approx \dot{r} + \omega r_s \cos\delta \sin(\alpha_g + \lambda - \alpha) \end{aligned} \tag{13}$$

where

r_s = station distance from 1 Earth's spin axis (spin radius)

z_s = stat ion height above Earth's equator (z.-hcight)

λ = station cast longitude

α_g = right ascension of Greenwich meridian

ω = Earth rotation rate (7,2921 15 x 105 rad/s)

r = geocentric spacecraft range

δ, α = spacecraft declination and right ascension, respectively

The range-rate signature is seen from Eq. (13) to contain two principal components, the geocentric spacecraft range rate, $\dot{r}$, and a sinusoidal variation ind uced by the diurnal motion of the station. For a spacecraft in a heliocentric orbit, the geocentric range rate changes slowly across several tracking passes, due to the bending of the spacecraft trajectory as viewed from J Earth. The significance of the diurnal range rate term in Doppler navigation, which provides an indirect measurement of the spacecraft's angular position on the celestial sphere, was first analyzed in detail by Hamilton and Melbourne [10], as wc]] as Curkendall and McReynolds [11]. Subsequently, Curkendall, along with McReynolds and Ondrasik, analyzed the mechanism by which the heliocentric bending of the spacecraft trajectory makes it possible for Doppler data to determine the

Earth-to-spacecraft range [11,12].

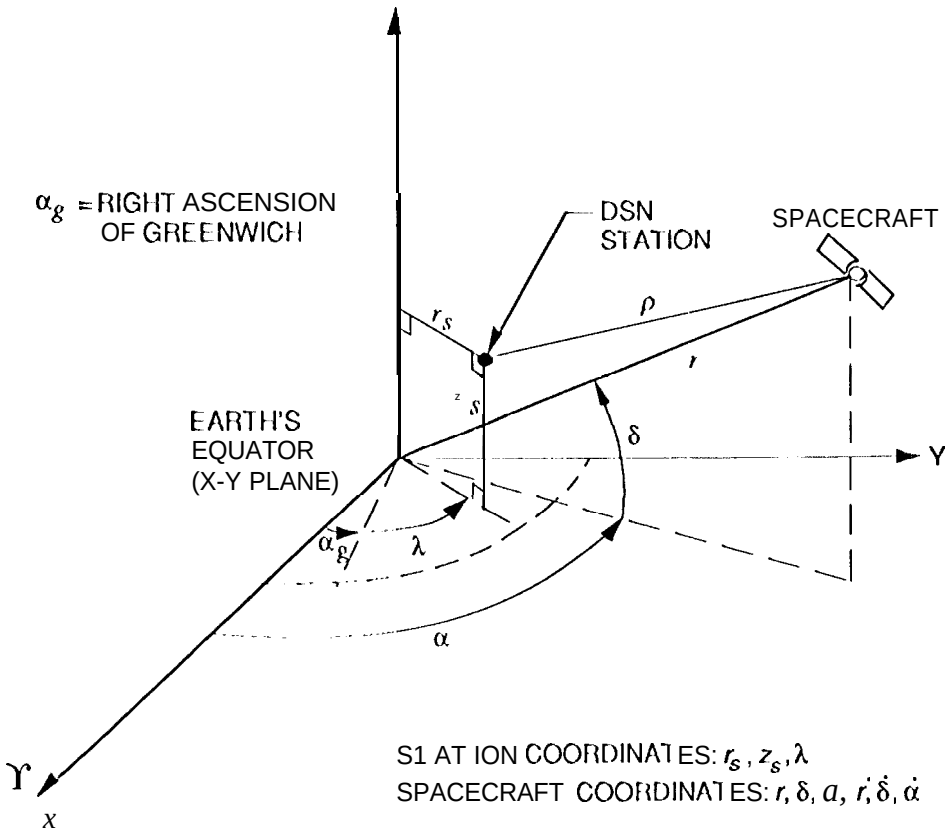

Fig. 2. Station-to-Spacecraft Tracking Geometry.

Ondrasik and Curkendall [12] developed an approximation of range rate that is suitable for navigation error anal ysis over periods of a few clays. 'l'heir expression gives the range rate as a function of six constant coefficients, a through f, that are funct ions of the spacecraft's six spherical coordinates at time t = O:

$$\dot{\rho} \approx a + b\sin \omega t + c\cos \omega t + d\omega t + e\omega t \sin \omega t + f\omega t \cos \omega t \tag{14}$$

where

$$
\begin{aligned}
a &= \dot{r}_0 - z_s\dot{\delta}_0\cos\delta_0 & d &= [\dot{r}_{g_0} + r_0(\dot{\delta}_0^2 + \dot{\alpha}_0^2\cos^2\delta_0)]/\omega \\
b &= \omega r_s\cos\delta_0 & e &= -\dot{\alpha}_0 r_s\cos\delta_0(\dot{\delta}_0\sin\delta_0 - \Lambda\alpha_0) \\
c &= -\omega r_s\Lambda\alpha_0\cos\delta_0 & f &= -\dot{\delta}_0 r_s\sin\delta_0(\dot{\alpha}_0\cos\delta_0 - \Lambda\alpha_0)
\end{aligned}
\tag{15}
$$

and

$\Lambda\alpha_0$ = difference between *a priori* and *actual* values of α_0

$\dot{r}_{g_0}$ = differential gravitational acceleration due to the Sun at $t = 0$

in Eq. (14), t is measured from a time at which the spacecraft nominally crosses the station's meridian. The theoretical precision, or information content, of a few passes of differenced-range Doppler data from a single station can be established by deriving an error covariance for the six data coefficients *a* through *f*, then treating these coefficients as "data points" from which an error covariance for the spacecraft coordinates at epoch can be obtained via Eq. (15). This approach has the advantage that the determination of the coefficients is independent of the tracking geometry.

An equivalent error analysis for counted Doppler can be constructed by using Eq. (14) to obtain an expression for the integrated range rate, $\Lambda\rho$, over a tracking pass beginning at time t_0, as a function of the same data coefficients *a* through *f*:

$$
\begin{aligned}
\Lambda\rho = \int_{t_0}^{t}\dot{\rho}dt &= a(t - t_0) + \frac{1}{\omega}(f - b)(\cos\omega t - \cos\omega t_0) + \frac{1}{\omega}(e + c)(\sin\omega t - \sin\omega t_0) \\
&+ \frac{d}{2}\omega(t^2 - t_0^2) - e(t\cos\omega t - t_0\cos\omega t_0) + f(t\sin\omega t - t_0\sin\omega t_0)
\end{aligned}
\tag{16}
$$

A direct comparison of differenced-range Doppler and counted Doppler can now be performed by using Eqs. (14) and (16) to derive the statistics of the six data coefficients given by Eq. (15) over

identical data arcs.

Using the measurement error models described previously, the error covariance for the data coefficients *a* through *f* was computed for two consecutive 8 hr tracking passes from a single station for both differenced-range Doppler and counted Doppler. The results are given in Table 2. in each case, it was assumed that no *a priori* information was available. Since the differenced-range Doppler measurement errors were assumed to be white, zero-mean, and Gaussian, the data coefficient covariance could be obtained by least-squares techniques, as described by Ondrasik and Curkendall [12]. For counted Doppler, a stochastic parameter must be estimated for each pass to represent both the phase offset, ϕ_0, and the accumulated phase noise induced by sources of frequency instability, in addition to the six data coefficients. This made it necessary to use a discrete sequential filter algorithm (a derivation of which is given by Bierman [13]) to obtain the error covariance.

Table 2 predicts that counted Doppler yields improvements in precision of 30 to 40 percent over differenced-range Doppler, despite the fact that phase-noise parameters must be estimated in addition to the spacecraft coordinates. The translation of the data coefficient uncertainties shown in Table 2 into spacecraft coordinate uncertainties requires the use of Eq. (1 S). If the gravitational acceleration is neglected for the sake of simplicity, then an approximate solution for the spacecraft coordinate uncertainties, originally developed by Curkendall and McReynolds [11], can be given as follows:

$$\sigma_{r_0} \approx \frac{\omega r_s^2}{v_\delta^2 + v_\alpha^2}\sigma_d \qquad \sigma_{\delta_0} \approx \frac{1}{\omega r_s |\sin \delta_0|}\sigma_b \qquad \sigma_{\alpha_0} \approx \frac{1}{\omega r_s \cos \delta_0}\sigma_c$$

$$\mathrm{CT}_v \approx \sigma_a \qquad \sigma_{v_\delta} \approx \frac{r_0}{r_s |\sin \delta_0|}\sigma_e \qquad \sigma_{v_\alpha} \approx \frac{r_0}{r_s}\sigma_f \tag{17}$$

where

$$(V_r, v_\delta, v_\alpha) = (\dot{r}_0, r_0\dot{\delta}_0, r_0\dot{\alpha}_0 \cos\delta_0) \qquad (18)$$

TABLE 2. Doppler Data Coefficient Uncertainties (8-hr Passes)

I Ma coefficient Uncertainty (1σ)	One Pass		Two Passes	
	Differenced-Range Doppler	Counted Doppler	Differenced-Range Doppler	Counted Doppler
a, mm/s	0.23	0.17	5.0×10^{-3}	3.4×10^{-3}
b, mm/s	3.3	2.6	1.7×10^{-3}	1.1×10^{-3}
c, mm/s	0.23	0.17	5.9×10^{-3}	4.0×10^{-3}
d, mm/s	2.2	1,7	$1,1 \times 10^{-3}$	0.76×10^{-3}
e, mm/s	0,12	0.09	0.38×10^{-3}	0.24×10^{-3}
f, mm/s	1.2	0,92	1.3×10^{-3}	0.89×10^{-3}

in Eq. (1 8), v_δ and v_α are the spacecraft velocity components that are normal to the Earth-to-spacecraft line of sight, in the direction of increasing declination and in the equatorial plane, respectively. Eq. (17) illustrates the dependence of 1 Doppler orbit determinat ion precision on the tracking geometry, in particular, the well-known indeterminacy that results in some coordinates when $\delta_0 = 0$. Doppler data are theoretically unable to sense the declination and the declination rate of a spacecraft that is crossing the celestial equator, although the indeterminacies predicted by Eq. (17) ate actually artifacts of the approximations used in the derivation of the formulas, and not genuine physical phenomena. It will be seen in the subsequent error covariance analysis that the

characteristics predicted by Eq. (17) are not necessarily accurate when longer data arcs (durations of weeks or months) arc employed.

Using the data coefficient uncertainties from Table 2, along with Eqs. (17) and (18), approximate spacecraft coordinate uncertainties were computed for the tracking geometry that existed for the *Mars Observer* spacecraft as it approached Mars, 30 days prior to arrival in late August 1993. The results are shown in Table 3. In performing the computations, it was assumed that the data were acquired by Deep Space Station (DSS) 15, the 34-m HEF station at the DSN complex in Goldstone, California ($r_s = 5204$ km). *Mars Observer* was supported exclusively by the 34-m HEF stations, which are the only DSN stations that presently support both uplink and downlink tracking at X-band frequencies.

TABLE 3. Results for Mars Observer Approach Geometry (Epoch 25 July 1993)
($r_0 = 3.2 \times 10^8$ km, $\delta_0 = 4.3$ deg, $v_\delta = -14.4$ km/s, $v_\alpha = 35.1$ km/s)

Spacecraft Coordinate Uncertainty (1σ)	One Pass		Two Passes	
	Differenced-Range Doppler	Counted Doppler	Differenced-Range Doppler	Counted Doppler
r_0, km	1.1×10^4	8.9×10^3	5.7	4.0
δ_0, μrad	1.2×10^2	93	0.06	0.04
α_0, μrad	0.60	0,42	0.02.	0.02
v_r, m/s	2.3×10^{-4}	1.7×10^{-4}	5.0×10^{-6}	3.4×10^{-6}
v& 111/s	100	77	0.31	0.19
v_α, m/s	71	56	0.08	0.05

For the geometry of Table 3, a 0.01-μrad angle translates into about 3.2 km in position normal to the Earth-to-spacecraft line. Radio-navigation accuracy for interplanetary spacecraft is often characterized by the uncertainty in the angular coordinates, which are normally the most poorly determined components of the trajectory. This is not always true for Doppler, though, because Doppler data, whether formulated as phase or frequency measurements, depend upon the centrifugal and gravitational acceleration of the spacecraft to determine range, as shown in Eq. (17). Remarkably, the theoretical angular precision of counted Doppler approaches that of ΔDOR, an interferometric data type used by *Mars Observer* and other missions that can measure the angular coordinates with a precision of about 0.03 μrad [14]. It must be remembered that the results in Table 3 include the effects of random measurement noise only, and that there are many other error sources affecting Doppler data that have not yet been addressed. The next section is devoted to a much more realistic error covariance analysis that incorporates all of the principal Doppler error sources.

Mars Observer Mission Scenario

The launch of *Mars Observer* on September 25, 1992 initiated the first interplanetary mission that was supported solely at X-band frequencies by the DSN. Most of the future missions that are currently planned, such as the *Mars Pathfinder* and the *Cassini* Saturn orbiter/Titan probe, will also be employing X-band tracking exclusively. To obtain a realistic indication of the potential navigation performance of X-band Doppler data, with both the current differenced-range Doppler formulation and the alternative counted Doppler formulation, an error covariance analysis of a navigation scenario derived from the *Mars Observer* interplanetary cruise phase was developed. This analysis is an outgrowth of an earlier study of X-band Doppler and ranging navigation accuracy by the authors that also utilized *Mars Observer*'s Earth-to-Mars transfer trajectory [15].

The interplanetary cruise phase of the mission extended from injection to initiation of the Mars Orbit Insertion (MOI) burn which was nominally scheduled for August 24, 1993; a duration of about 11 months. Although communication with the spacecraft was tragically lost just days prior to MO], the interplanetary cruise phase of the mission represented a challenging navigation scenario, as the declination of the *Mars Observer* at encounter was within 1 deg of zero. This is a geometry which has historical] y yielded relativel y poor performance with Doppler tracking, due to Doppler data's relative insensitivity to some components of the spacecraft's state in this regime. The cruise period was segmented for mission planning purposes into five subphases, each ending prior to a planned trajectory correction maneuver, The trajectory segment used in this analysis was the fourth subphase, a 182-day time period from early February 1993 to early August 1993, which represents the longest leg of the interplanetary cruise, and had the most stringent navigation accuracy requirements, in order to support the final maneuver prior to MO], Over the time span of the data arc, the Rarth-to-spacecraft range varied from 80×10^6 to 330×10^6 km, while the geocentric declination of the spacecraft ranged from 22 deg to 1 deg. The Sun-l{arth-probe angle over this period varied from 125 deg to 45 deg. Using this trajectory segment, orbit determinat ion error statistics were computed for a DSN Doppler data set processed using either a differenced-range Doppler formulation of the data, or a counted Doppler formulation, then propagated to the time of MO] and displayed in a Mars-centered aiming plane (B-plane) coordinate system.[4]

Two-way X-band Doppler passes were simulated from injection plus 143 (1+143) days to I+325 days; MO] would have nominally occurred at I+337 days, The data were assumed to be acquired from the DSN'S 34-111 HEF stations located near Gold stone, California (DSS 15),

[4]The aiming plane, or B-plane, coordinate system is dc.fine.d by three unit vectors, $\underline{S}$, $\underline{T}$, and $\underline{R}$; $\underline{S}$ is parallel to the spacecraft velocity vector relative to Mars at the time of entry into Mars' gravitational sphere of influence, $\underline{T}$ is parallel to the Martian equatorial plane, and $\underline{R}$ completes an orthogonal triad with $\underline{S}$ and $\underline{T}$. The aim point for a planetary encounter is defined by the miss vector, B, which lies in the $\underline{T}$-$\underline{R}$ plane, and specifics where the point of closest approach would be if the target planet had no mass and did not deflect the. flight path.

Canberra, Australia (DSS 45), and Madrid, Spain (DSS 65). From I+143 to 1+247 days, one horizon-to-horizon pass was acquired each clay from DSS 65. From I-I 2.47 to I+307 days, two passes were acquired on a daily basis, from D SS 65 and DSS 45. From I+307 to I+325 days, data were acquired continuously, utilizing all three sites.]n all cases, the Doppler data were collected at a rate of one point every 10 minutes. The data noise modeling assumptions of 'l'able 1 were used to represen t the differenced-range Doppler and counted Doppler random measurement errors. For both Doppler formulations, the additive noise variances were adjusted by an elevation-dependent function for all stations, to reduce the weight of the low-elevation data, Furthermore, no data were acquired at elevations of less than 10 deg.

Orbit Determination Filter Model

The filter model used in this analysis is summarized in Table 4. The filter parameters were grouped into three categories: spacecraft epoch state, spacecraft non gravitational force mode], and ground system error model. The ground system error model included random biases representing station location errors, and stochastic parameters representing Earth orientation and station-dependent tropospheric zenith delay calibration errors. The remaining ground system parameters, which represented station-dependent ionospheric zenith delay calibration errors, were not included in the filter, but were modeled as consider parameters whose effects were incorporated into the error covariance of the fil ter parameters. The nongravitat ions] force model contained parameters representing solar radiation pressure, as well as small anomalous forces due to gas leaks from valves and pressurized tanks, attitude control thruster misalignments, etc. The error covariance matrix for the filter parameters was computed using a sequential *U-D* factorized filter algorithm, as described by Bierman [13]. The effects of uncertainty in the ephemeris and mass of Mars were neglected, as they were relatively small in this particular scenario.

TABLE 4. *Mars Observer* Orbit Determination Filter Model

Estimated Parameter Set	Uncertainty(1σ)	Remarks
Spacecraft Epoch State	*a priori*,	constant parameters
position components	10^5 km	
velocity components	1 km/s	
Nongravitational Force Model		
solar radiation pressure:	*a priori*,	constant parameters
radial (G_R)	10% (= *0.13*)	
transverse (G_X/G_Y)	10% (=0.01)	
anomalous accelerations:	steady-state,	Markov parameters,
radial (a_R)	10-12 km/s^2	lo-day time constant
transverse (a_X/a_Y)	10^{-12} km/s^2	lo-day time constant
Ground System Error Model		
DSN station locations:	*a priori*,	constant parameters,
spin radius (r_s)	*o.]* 8 m	relative uncertainty
z-height (z_s)	0.23 m	between stations is
longitude (λ)	3.6 x 10^{-8} rad	1 to 2 cm
Earth orientation:	steady-state,	Markov parameters
pole orientation	1.5 x 10^{-8} rad	1-day time constant
rotation period	0.2 ms	12-hr time constant
phase offsets (one per station per pass, counted Doppler only)	*a priori*,	random walk
ϕ_0	100 km	N = 1 cm^2/hr
transmission media:	*a priori*,	random walk,
zenith troposphere (each station)	5 cm	N = 1 cm^2/hr
Consider Parameter Set		
zenith ionosphere (each station)	3 cm	constant parameters, X-band value

For the *Mars Observer* solar radiation pressure. model, three nondimensional coefficients representing a simple spacecraft bus model (G_R, G_x, G_Y) were est imated, with a *priori* uncertainties equivalent to 10 percent of their nominal values (see "l'able 4). The coefficient G_R represents the solar radiation pressure component along the Sun-to-spacecraft line, while the other two orthogonal components normal to this line arc represented by the G_X and G_Y coefficients. Spacecraft anomalous accelerations in each body-fixed axis direction were modeled as exponent i all y correlated process noise (first-order M arkov processes), as shown in 'l'able 4, For these accelerations, the same conventions were used as for the solar radiation pressure coefficients: in Table 4, the parameter a_R represents the acceleration acting along the Sun-to-spacecraft line, while the other two accelerations, a_X and a_Y, act along the two orthogonal directions that are both normal to this line.

The 34-m HEF station location errors were assumed to bc constant in the Earth-fixed frame over the time span of the data arc. This implies that movement of the stations due to such phenomena as solid Earth tides and plate motion must be properly calibrated at the 1 to 2 cm level, in order for the assumptions given herein to bc valid, The station location uncertainties given in '1'able 4 are based upon a station location set developed by Finger and Folkner [16] from a comparison of Earth orientation measurements made with Very Long Baseline Interferometry (V].]]]) observations of extragalactic radio sources and with Lunar laser ranging data. The formal covariance obtained by Finger and Folkner has been adjusted to account for uncertainties in the location of the geocenter (as determined from Lunar laser ranging and satellite laser ranging measurements), the orientation of the radio ant] planetary ephemeris coordinate frames, and calibrations of the Earth's pole location and rotation period. To account for dynamical uncertainties in the location of the Earth's pole and the Earth's rotation period, collectively referred to as Earth orientat ion, three additional exponentiall y correlated process noise parameters were included in the filter.

The tropospheric path delay calibration error at each station was modeled as a Brownian motion ("random walk") process. In "l'able 4, N demotes the noise density of this process. The tropospheric zenith delay was modeled in this manner to account for day-to-day variations relative to a seasonal model used to calibrate the Doppler data, and for errors induced in mapping the zenith delay values to the station-to-spacecraft line of sight. in the future, tropospheric calibrations derived from space-based geodetic systems such as VI .BI or Global Positioning System (GPS) satellite tracking data should yield substantially smaller calibration errors than those assumed herein. It was not thought that an adequate filter model for the effect of ionospheric path delay calibration errors on the data could be postulated, as the behavior of the ionosphere is highly dependent upon the location and movement of the Sun with respect to the station-to-spacecraft line of sight, as well as other elevation-dcpcndcnt parameters. Therefore, the zenith ionospheric calibration errors at each station were treated as consider parameters with an uncertainty of 5.0 x 1016 electrons/m^2 (equivalent to about 3 cm). This level of uncertaint y incorporates the effects of mapping errors in add it ion to the zenith delay cal i brat ion error,

in the counted Doppler cases, a phase offset parameter for each station was included in the ground system error model. As with tropospheric path delays, these parameters were modeled as random walk processes. The noise density, N, given for these parameters in 'J'able, 4 was derived from the value of σ_w given in '1'able 1 for the white frequency noise that represents ground system frequency instability and uncalibrated solar plasma variations. The covariance matrix entries for each of these parameters were reset after each station pass, since the Doppler counter initialization procedure at each station effectively yields a new phase offset for each pass.

Results

The error covariance analysis results are summarized in Tables 5 and 6. "1'able 5 gives the dimensions of the B-plane dispersion ellipses around the nominal MOI aim point for both Doppler formulations, and Table 6 gives aim-point position uncertainties in the time-of-flight direction, which is in the $\underline{S}$ axis direction, normal to the B-plane. The data in Tables 5 and 6 are broken down into cases in which error covariance computations were performed using on] y subsets of the total parameter set described in Table 4, as well as the case in which the complete model of "l'able 4 was used. The B-plane dispersion ellipses obtained with differenced-range Doppler and counted Doppler for the full parameter set are illustrated in Fig. 3, which also indicates the approximate directions to the Earth, the Sun, and Mars at the time of arrival, As *Mars Observer* approached Mars, its flight path was within about 15 deg of being perpendicular to the Earth-to-Mars line; therefore, the direction to the Earth shown in Fig. 3 is inclined about 1S deg to the IJ-plane. The direction to the Sun that is shown in Fig. 3 very nearly lies in the n-plane, to within about 2 deg. The directions to both the Earth and the Sun lie in the plane of the ecliptic. "l'he dispersions in Tables 5 and 6 correspond to a geocentric angular uncertaint y of about 0.04 μrad for both Doppler formulations, which is close to the theoretical results of 'l'able 3.

Figure 3 illustrates the principal differences between the performance of the Doppler data processing modes: 1) the proposed fil tering strategy yielded superior accuracy results over the traditional filtering strategy for differenced-range Doppler, and 2) the Earth-to-spacecraft range component of the MO] aim point was determined much more accurately with counted Doppler than with differenced-range Doppler. Counted 1 Doppler did not yield an y improvement in accuracy in the time-of-flig}]t direction, however, and in the direction normal to the Earth-to-spacecraft line of sight that lies in the B-plane. '] 'ables 5 and 6 also illustrate the impact of having to estimate phase offset parameters for each pass when using counted Doppler. In the two cases in which these phase offsets were not included ("state only" and "state plus nongravitational force model"), the performance of counted Doppler was proportionally much better than the performance of

differenced-range Doppler than in the cases in which the ground system error model was present,

TABLE 5. *Mars observer* Aim-Point Dispersions (B-plane)

Parameter Set	*B*-Plane Dispersion Ellipse Dimensions (1 σ, km)	
	Differenced-Range Doppler	Counted Doppler
State only	*0,50 x 0.04*	$6.8 \times 10^{-4} \times 3.4 \times 10^{-7}$
State plus Ground System Error Model	3.8 x 0,36	0.78 X 0.26
State plus Non-Gravitational Force Model	84 x 9.4	2.() x *0.44*
All	94 x 24	28 × 12

TABLE 6. *Mars Observer* Aim-Point Dispersions (Time Of Flight)

Parameter Set	Time-of-Flight Position Uncertainty (1 σ, km)	
	Differenced-Range Doppler	Counted Doppler
State Only	o.15	1.7×10^{-4}
State plus Ground System Error Model	1,0	0.19
State plus Non-Gravitational Force Model	4.8	1.0
All	13	13

To investigate the sensitivity of the orbit determination accuracies obtained with differenced-range Doppler and counted Doppler to the accuracy of these measurements, computations were performed for an additional case with degraded data accuracies. in this case, which utilized the full

parameter set of Table 4, the data sigmas given in 'l'able 1 were increased by a factor of 10; results are summarized in Table 7. The aim-point dispersions in the degraded data case were found to be 20 to 40 percent larger than those obtained with the baseline data accuracies; the orientations of the B-plane dispersion ellipses were virtually unchanged from those shown in Fig. 3. An examination of the error covariance matrices obtained in the degraded data case versus those obtained with the baseline data accuracies revealed that the uncertain ics of all of the filter parameters were increased fairly uniformly when the data were deweighted. These results suggest that the performance of both Doppler formulations is determined more by uncertainty in the nongravitational force model and ground system error model parameters, rather than by the accuracy of the data. To some extent, this behavior is desirable, as it indicates that the filter possesses some robustness with respect to errors in the assumed data accuracies.

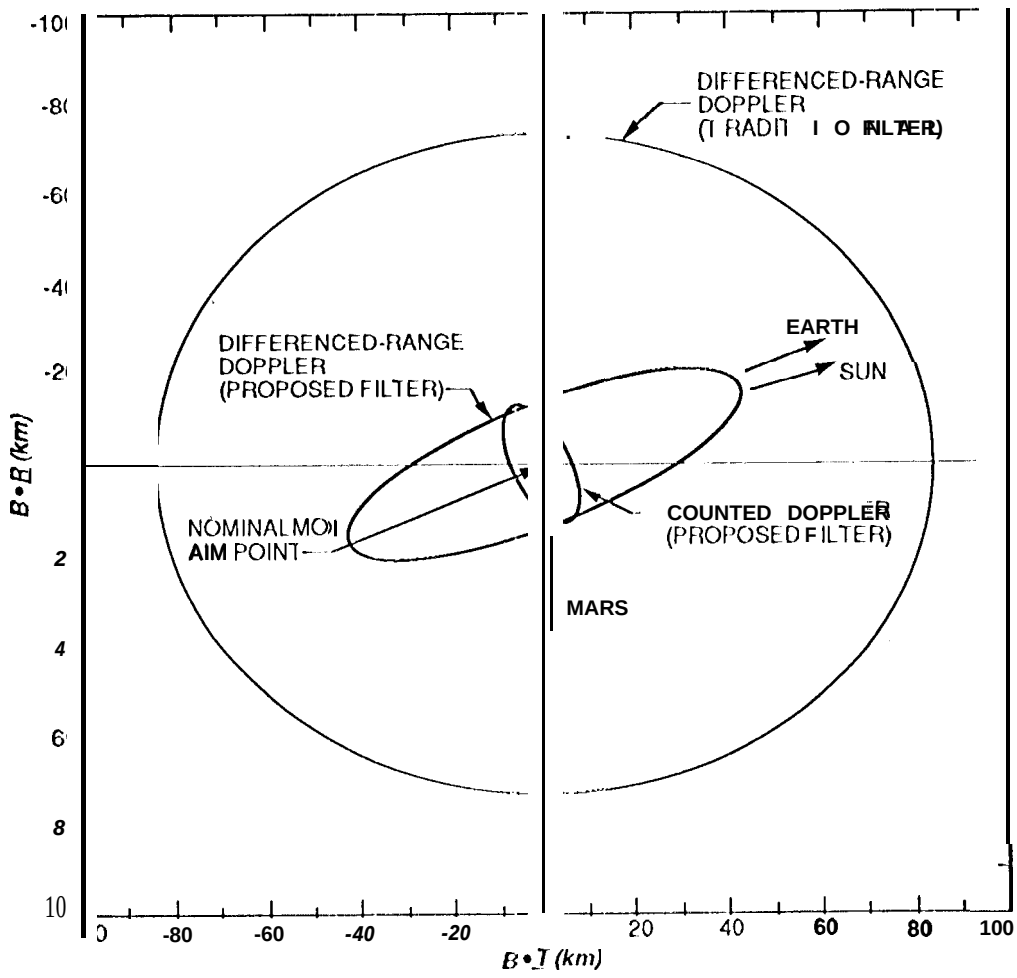

Fig. 3. Mars-Centered B-Plane Dispersion Ellipses (1 σ)

TABLE 7. Results for Degraded (x1O) Data Cases

Data Formulation	Aim-Point Dispersions (1 σ, km)	
	B-Plane	Time of Flight
Differenced-Range Doppler	106 × 36	18
Counted Doppler	34 × 12	15

Discussion

The results of this study, if they can be realized in practice, are quite remarkable, as they predict that navigation accuracies which previously required the use of additional data types might be achieved with only a more sophisticated treatment of Doppler. With a filter of the type used by the authors in their earlier analysis of a similar *Mars Observer* scenario [15], the best performance predicted for differenced-range Doppler data consisted of a B-plane dispersion ellipse (1 σ) of 166 x 146 km, and a time-of-flight position uncertainty (1 σ) of 59 km. These dispersions were heavily influenced by unmodeled tropospheric path delay and station location calibration errors, as the filter employed did not contain a ground system error model, but treated those error sources as consider parameters. 'l'he results obtained herein for differenced-range Doppler indicate a factor of two to four improvement over the previous study, while the counted Doppler results correspond to almost an order of magnitude improvement (see Fig. 3). Another point of comparison is an analysis performed for the *Mars Observer* mission by Roth [17], who found that the predicted MO] aim-point dispersions, using X-band two-way differenced-range Doppler, two-way ranging, and ΔDOR data, are a B-plane dispersion ellipse (1σ) of 40 x 4 km, and a time-of-flight position uncertainty (1 σ) of 26 km. These statistics include uncertainty in the Martian ephemeris, which is about 10 km in position relative to the Earth at the time of at-rival. As in all previous interplanetary missions, the orbit determination filter that was used operationally for *Mars Observer* did not incorporate a ground system error model.

in the *Mars Observer* scenario, the principal advantage of counted Doppler was its ability to estimate solar radiation pressure: the uncertainty in the radial solar pressure coefficient, G_R, was reduced from an *a priori* uncertaint y of 10 percent of its nominal value to about 2 percent with counted Doppler, whereas differenced-range 1 Doppler reduced this uncertainty to only about 6 percent.]n this regard, counted Doppler's ability to estimate the Ilarlh-to-spacecraft range (and

hence accelerations in this direction) was much better relative to differenced-range Doppler than the theoretical predictions indicated. With both Doppler formulations, the station location uncertainties were reduced from about 20 cm down to 3 to 12 cm, the larger uncertainties being in the station z-height coordinates; the tropospheric zenith delay uncertainties remained at or near their *a priori* values of 5 cm. The filter's ability to correct the station locations was found to be limited by the uncertainty in the parameters representing Earth orientation calibration errors, which were not improved very much by either Doppler formulation. It should be noted that with the exception of the phase offset parameters in the counted Doppler cases, the primary reason for representing ground system calibration error sources as filter parameters was not to reduce their uncertainties, but to make these uncertainties known to the filter as it constructed an estimate of the spacecraft trajectory. Admittedly, the performance of such a filter must be validated with actual data prior to any operational use.

in the past, one of the principal obstacles to the operational use of counted Doppler data was perceived to be the presence of discontinuities in the Doppler phase known as *cycle slips*, which occur when the ground receiver's phase tracking loop momentarily loses its lock on the spacecraft carrier signal. Cycle slips most often occur when the spacecraft's Doppler frequency is large and varies rapidly, as in the case of a low-altitude planetary orbiter, or when the spacecraft carrier signal-to-noise ratio approaches the tracking threshold of the ground receiver, a highly unstable regime of operation. in this analysis, it was implicitly assumed that cycle slips in the ground station receivers were infrequent, and that any cycle slips that did occur were identified and corrected. For a spacecraft in interplanetary space this is thought to be a reasonable set of assumptions, as the principal source, of Doppler frequency variations for such vehicles is the diurnal motion of the station, which can be tracked very accurately by modern DSN receivers. Identifying and removing the occasional cycle slip that might occur under these circumstances should not be a difficult task,

Summary And Conclusions

This study investigated different approaches for improving X-band Doppler navigation accuracy for interplanetary spacecraft. A simple analysis found that a phase formulation of Doppler data, known as counted Doppler, is theoretically capable of sensing the geocentric motion of a distant spacecraft with roughly 30 to 40 percent greater precision than the quasi-frequency Doppler formulation known as differenced-range Doppler, currently in use. In a detailed error covariance analysis of a *Mars Observer* interplanetary cruise scenario, it was found that an orbit determination filter containing models for the principal ground system calibration error sources may yield much better performance than a filter that does not model these error sources. With this filter, both Doppler formulations were able to predict the angular coordinates of the spacecraft's Mars orbit insertion aim point with an accuracy (1 σ) of about 0.05 rad (15 km in position). The principal difference between the two cases was that the Earth-to-spacecraft range at arrival was determined with an accuracy (1 σ) of about 6 km with counted Doppler, a factor of eight better than with differenced-range Doppler. In general, the results suggest that X-band Doppler navigation accuracy for interplanetary spacecraft is determined more by the magnitude and character of the spacecraft nongravitational forces and the filtering strategy used m reduce the data, rather than the performance of the DSN Doppler system.

Acknowledgments

The authors extend their thanks to J. C. Breidenthal, W. M. Folkner, R. A. Jacobson, S. M. Lichten, J. K. Miller, and X X Newhall for lending their time and expertise to this effort. The research described in this article was performed at the Jet Propulsion Laboratory, California Institute of Technology, under contract with the National Aeronautics and Space Administration.

References

[1] MOYER, T. D., *Mathematical Formulation of the Double-Precision Orbit Determination Program*, Technical Report 32-1527, Jet Propulsion Laboratory, Pasadena, California, May 1971, pp. 72-80.

[2] JORDAN, J. F., and WOOD, 1., J., "Navigation, Space Mission," *Encyclopedia of Physical Science and Technology,* Vol. 8, Academic Press, inc., New York, 1987, pp. 744-767.

[3] CURKENDALL, D. W., "Orbit Accuracy as a Function of Doppler Sample Rate for Several Data Taking and Processing Modes," *JPL Space Programs* **Summary** *37-.?8,* Vol. II 1, Jet Propulsion Laboratory, Pasadena, California, January- February 1966, pp. 20-24.

[4] MILLER, J. K., "The Effect of Clock, Media, and Station location Errors on Doppler Measurement Accuracy," *The Telecommunications and Data Acquisition Progress Report 42-1 l.?,* Vol. January- March 1993, Jet Propulsion Laboratory, Pasadena, California, June 1992, pp. 7-21.

[5] Deep *Space Network/Flight Project Interface Design Handbook Vol. 1: Existing DSN Capabilities,* JPL Internal Document 810-5, Rev. D, Module TRK-20, Rev. D, Jet Propulsion 1.aboratory, Pasadena, California, March 1990, pp. 7-21.

[6] CURKENDALL, D. W., *Problems in Estimation Theory with Application to Orbit Determination*, Report UCLA-ENG-7275, UCLA School of Engineering and Applied Science, University of California, Los Angeles, September 1972, pp. 7-25.

[7] KWOK, A., "DSS 15 X-hand Closed-loop System Frequency Stability," JPL interoffice Memorandum 3393-91-() 17 (internal document), Jet Propulsion Laboratory, Pasadena, California, January 1991.

[8] *Deep Space Network/Flight Project Interface Design Handbook Vol. 1: Existing DSN Capabilities,* Module FTS- 10, Rev. A, Jet Propulsion Laboratory, Pasadena, California, July 1991, pp. 3-9.

[9] ARMSTRONG, J. W., WOO, R. AND ESTABROOK, F. B., "Interplanetary Phase Scintillation and the Search for Very Low Frequency Gravitational Radiation," *The Astrophysical Journal,* Vol. 230, June 1979, pp. 570-574.

[10] HAMILTON, "J'. W., and MELBOURNE, W, G., "Information Content of a Single Pass of Doppler Data from a Distant Spacecraft ," *JPL Space Program Summary 37-.?9, Vol. III*, Jet Propulsion Laboratory, Pasadena, California, March-April 1966, pp. 18-23.

[11] CURKENDALL, D. W., and MCREYNOLDS, S. R., "A Simplified Approach for Determining the information Content of Radio Tracking Data," *Journal of Spacecraft and Rockets*, Vol. 6, No. 5, May 1969, pp. 520-525.

[12] C) DRASIK, V. J. AND CURKENDALL, D. W., "A lJirst-Order Theory for Use in investigating the information Content Contained in a Few Days of Radio Tracking Data," *The* Deep *Space Network l'regress Report*, 'J'ethnical Report 32-1526, Vol. 111, Jet Propulsion Laboratory, Pasadena, California, June 1971, pp. 77-93.

[13] BIERMAN, G. J., *Factorization Methods for Discrete Sequential Estimation,* Academic Press, inc., Ncw York, 1977, pp. 19-24 and 135-182.

[14] BORDER, J. S., "Analysis of ADOR and ADOD Measurement Errors for *Mars Observer* Using the DSN Narrow Channel Bandwidth VLBI System," JPL Interoffice Memorandum 335.1-90-026 (internal document), Jet Propulsion 1.aboratory, Pasadena, California, May 1990.

[15] ESTEFAN, J, A., and THURMAN, S. W., "Precision X-Band Radio Doppler and Ranging Navigation: Mars Observer interplanetary Cruise Scenario," *The Telecommunications and Data Acquisition Progress Report 42-111,* Vol. July- September 1992, Jet]'repulsion Laboratory, Pasadena, California, November 1992, pp. 11-22.

[16] FINGER, M, 11., and FOLKNER, W. M., "A Determination of the Radio-Planetary Frame Tie 1 'rem Comparison of Earth Orientation Parameters," *The Telecommunications and Data Acquisition Progress Report 42-109*, Vol. January- March 1992, Jet Propulsion Laboratory, Pasadena, California, May 1992, pp. 1-21.

[17] ROTH, D. c., "Mars Observer ΔDOR Requirements from MOI-90 days to MO]," JPL Interoffice Memorandum MO-NAV-92-080 (internal document), Jet Propulsion 1.aboratory, Pasadena, California, September 1992.